CHEMISTRY OF MATERIALS

ARTICLE

pubs.acs.org/cm

N,N-Di*aryl*anilinosquaraines and Their Application to Organic Photovoltaics

Siyi Wang,[†] Lincoln Hall,[†] Vyacheslav V. Diev,[†] Ralf Haiges,[†] Guodan Wei,[‡] Xin Xiao,[‡] Peter I. Djurovich,[†] Stephen R. Forrest,[‡,§] and Mark E. Thompson*[,†]

[†]Department of Chemistry, University of Southern California, Los Angeles, California 90089, United States

[‡]Department of Materials Science and Engineering, University of Michigan, Ann Arbor, Michigan 48109, United States

[§]Departments of Electrical Engineering and Computer Science and Physics, University of Michigan, Ann Arbor, Michigan 48109, United States

Supporting Information

ABSTRACT:

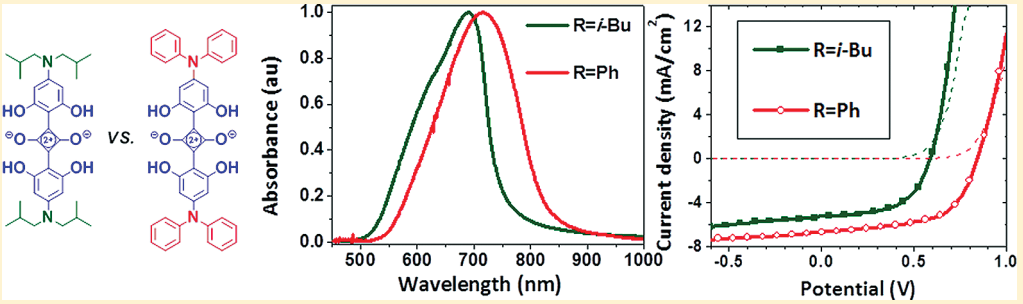

We report new derivatives of symmetric squaraine dyes with N,N-di*aryl*anilino substituents that have high solubility and high absorptivity (ε = 0.71−4.1 × 10^5 M^{-1} cm^{-1}) in the red solar spectral region (λ_{max} = 645−694 nm) making them promising candidates for application in organic photovoltaics (OPVs). Unsymmetrical N,N-diisobutylanilino- and N,N-diphenylanilino-(diphenylamino)squaraines have also been prepared that give blue-shifted absorption spectra (λ_{max} = 529−535 nm) relative to their symmetric counterparts. Compared to bis(N,N-diisobutylanilino)squaraine, both symmetrical and unsymmetrical N,N-di*aryl*anilino squaraines show markedly broader absorption bands in solution than their N,N-di*alkyl*anilino squaraine counterparts: the full width at half-maximum (fwhm) for N,N-di*aryl*anilino squaraines range from 1280−1980 cm^{-1}, while the fwhm value for the N,N-diisobutylanilino squarine is only 630 cm^{-1}. The absorption bands for thin films of N,N-di*aryl*anilino squaraines broaden further to 2500−3300 cm^{-1}. N,N-Di*aryl*anilino squaraines are fluorescent, albeit with lower quantum yields than bis(N,N-diisobutylanilino)squaraine (ϕ_{PL} = 0.02−0.66 and 0.80, respectively). OPVs were prepared with solution processed squaraine layers using the following structure: ITO/squaraine (66−85 Å)/C_{60} (400 Å)/BCP (100 Å)/Al (1000 Å), BCP = bathocuproine. Devices using thin films of the bis(N,N-di*aryl*anilino)squaraines as donor layers show improved performance relative to OPVs prepared with bis(N,N-di*alkyl*anilino)squaraines, i.e. bis(N,N-diisobutylanilino)squaraine: open-circuit voltage V_{oc} = 0.59 ± 0.05 V, short-circuit current J_{sc} = 5.58 ± 0.16 mA/cm^2, fill factor *FF* = 0.56 ± 0.03, and power conversion efficiency η = 1.8 ± 0.2% under 1 sun, AM1.5G simulated illumination, compared with bis(N,N-diphenylanilino)squaraine: V_{oc} = 0.82 ± 0.02 V, J_{sc} = 6.71 ± 0.10 mA/cm^2, *FF* = 0.59 ± 0.01, and η = 3.2 ± 0.1%. Morphological studies of thin films suggest that the solubility of bis(N,N-di*aryl*anilino)squaraines plays an important role in controlling the optoelectronic properties of the OPVs.

KEYWORDS: squaraine dyes, organic photovoltaic, solar cell,

INTRODUCTION

Squaraine dyes give rise to intense absorption in the red (600−700 nm) and near-infrared (NIR) spectral regions,[1,2] making them excellent candidates for a range of potential applications such as xerographic photoreceptors,[3−5] optical recording,[6] nonlinear optics,[7] photodynamic therapy,[8,9] bioimaging,[10] and solar energy conversion.[11−18] In previous work we have used bis(N,N-di*alkyl*anilino)squaraines as a donor material in organic photovoltaics (OPVs)[19−21] achieving efficiencies as high as 5.5%.[22] However, there are several drawbacks associated with the bis(N,N-di*alkyl*anilino)squaraines that limit their performance in OPVs: poor solubility unless substituted with large alkyl groups, absorption bands mainly in the red and NIR requiring other materials to achieve broadband response, and

Received: July 20, 2011
Revised: September 26, 2011
Published: October 18, 2011

low charge carrier mobility. The presence of N,N-dialkyl groups, while necessary to produce soluble squaraines, can hinder charge carrier transport.[14,23] Fortunately, incorporation of N-aryl groups in alkylamines has been shown to improve the charge and exciton transport properties in films due to enhanced intermolecular $\pi-\pi$ overlap.[24,25] By analogy, replacing the N-alkyl groups of anilinosquaraines with N-aryl moieties should improve both charge and exciton transport and, moreover, allow for tuning of the absorption profile and the molecular frontier orbital energy levels, which can result in tuning of the open circuit voltage (V_{oc}). To our knowledge there have not been any reports to date of simple anilinosquaraines appended with N-aryl substituents. Here, we demonstrate a facile synthesis of both symmetric bis(N,N-di*aryl*anilino)squaraines and unsymmetrical anilino(diphenylamino)squaraines that are soluble and have tunable absorption profiles and orbital energetics. Single crystal X-ray analysis of one derivative, bis(N,N-diphenylanilino)squaraine **3**, shows a π-stacking packing arrangement that is conducive for intermolecular charge transport. Relative to N-alkylanilino squaraines, the symmetric N-aryl analogs show significant differences in their absorption and emission properties. Bilayer photovoltaic devices fabricated using the symmetric anilinosquaraines as solution-processed donors indicate that the N-aryl substituents can improve the open-circuit voltage, charge transport, and overall performance of OPVs.

EXPERIMENTAL SECTION

Instrumentation. *General.* NMR spectra were recorded on Varian Mercury 500 MHz spectrometers at room temperature and 60 °C. Mass spectral analysis was performed on a Shimadzu Prominance-LCMS 2020 equipped with a column oven (T = 40 °C), a PDA photodetector (200−800 nm), and an MS spectrometer (LCMS 2020; m/z range: 0−2000; ionization modes: ESI/APCI). Thermogravimetric analyses were performed using a thermogravimetric analyzer TA Q50 (TA Instruments) under a high-purity air flow (80 mL min^{-1}). Samples were heated from 30 to 600 °C at a linear rate of 10 °C min^{-1}. UV−visible spectra were recorded on a Hewlett-Packard 4853 diode array spectrophotometer. Steady-state emission experiments at room temperature were performed using a Photon Technology International Quanta Master Model C-60SE spectrofluorimeter. Quantum efficiency measurements were carried out using a Hamamatsu C9920 system equipped with a xenon lamp, calibrated integrating sphere, and model C10027 photonic multichannel analyzer.

Electrochemistry. Cyclic voltammetry (CV) and differential pulse voltammetry (DPV) were performed using an EG&G potentiostat/galvanostat model 263 under N_2 atmosphere. Anhydrous DCM was used as solvent for the scan from −2 to 2 V and 1.0 M tetrabutylammonium hexafluorophosphate (TBAH) was used as the supporting electrolyte. A glassy carbon rod was used as a working electrode, and a silver wire was used as a pseudoreference electrode. Electrochemical reversibility and redox potentials were determined using CV and DPV, respectively. The redox potentials were calculated relative to an internal ferrocenium/ferrocene (Fc^+/Fc) reference.

Ultraviolet Photoemission Spectroscopy Measurements. The highest occupied molecular orbital (HOMO) energy of squaraines **3**, **4**, **5**, **9**, and **10** were measured by ultraviolet photoemission spectroscopy (UPS). Thin films of squaraines (20 Å) were spin-cast on the top of ITO coated glass substrates in an inert N_2 environment (H_2O < 1 ppm, O_2 < 5 ppm). The samples were then transferred in a sealed N_2-filled case to the ultrahigh vacuum analysis chamber (base pressure <3 × 10^9 Torr) without exposure to air. UPS data of each squaraine sample were collected using the 21.22 eV He(I) emission from a gas discharge lamp and a Thermo VG Scientific CLAM4MCD electron energy analyzer with a pass function full width at half max of 0.16 eV. Samples were biased at −9 V to ensure collection of the lowest kinetic energy electrons in order to accurately determine the photoemission cutoff and the vacuum level at the sample. The HOMO level was determined by the intersection of the background with a linear fit to the rising edge of the shallowest binding energy states.

X-ray Crystallography. A metallic green prism-like crystal of **1** obtained from CH_2Cl_2/MeOH was used for the X-ray crystallographic analysis. The X-ray intensity data were measured on a Bruker SMART APEX diffractometer equipped with an APEX CCD system and a Mo sealed-tube fine-focus source (λ = 0.71073 Å). A total of 1850 frames were collected over a total exposure time of 10.3 h. The frames were integrated with the Bruker SAINT V6.02A software package using a narrow-frame algorithm. The calculated minimum and maximum transmission coefficients (based on crystal size) are 0.782 and 0.983. The X-ray crystallographic analysis for **3** was performed on a metallic green-blue plate-like specimen obtained from toluene. The X-ray intensity data were measured on a Bruker SMART APEX DUO diffractometer equipped with a APEX II CCD system and a Cu ImuS microfocus source (λ = 1.54178 Å). A total of 2764 frames were collected over a total exposure time of 69.10 h. The frames were integrated with the Bruker SAINT V7.68A software package using a narrow-frame algorithm. The calculated minimum and maximum transmission coefficients (based on crystal size) are 0.6087 and 0.7516. Both structures were solved and refined using the Bruker SHELXTL V6.12 software package. Additional refinement details and the resulting factors for **1** and **3** are given in Table 1 and the Supporting Information.

Device Fabrication. Photovoltaic cells were grown on ITO-coated glass substrates that were solvent cleaned and treated in UV-ozone for 10 min immediately prior to loading into a high vacuum (base pressure ~3 × 10^{-6} Torr) chamber. The C_{60} (MTR limited) and 2,9-dimethyl-4,7-diphenyl-1,10-phenanthroline (BCP) (Aldrich) were purified by thermal gradient sublimation in vacuum prior to use. The metal cathode material, Al (99.999% pure, Alfa Aesar), was used as received. The squaraine films were spin-cast in air at 3000 rpm for 40 s on precleaned ITO substrates from 1 mg/mL chloroform solutions. The resultant films had the following thickness: SQ **1** 85 Å (±5 Å), SQ **3** 85 Å (±5 Å), SQ **4** 85 Å (±5 Å), and SQ **5** 66 Å (±1 Å). The squaraine films were transferred to a high vacuum chamber for deposition of C_{60} and BCP by vacuum thermal evaporation at the following rates: C_{60} (2 Å/s) and metals: 1000 Å thick Al (3 Å/s). The cathode was evaporated through a shadow mask with an array of 1 mm diameter openings.

Current−voltage measurements were performed in ambient using a Keithley 2420 SourceMeter in the dark and under corrected 1 kWm^{-2} white light illumination from a 300 W Xe arc lamp (Newport Oriel Product Line) equipped with an AM 1.5G filter. The current−voltage characteristics are reported from the average performance of several contacts made from individual devices. Spectral mismatch correction was performed as described in the literature,[26−28] using a Si photodiode (Hamamatsu S1787-04; 8RA filtered or S1787-12; KG5 filtered), calibrated at the National Renewable Energy Laboratory (NREL), and frequency modulated illumination (250 Hz) from a Xe source coupled to a Cornerstone 260 1/4 M monochromator (Newport 74125) in conjunction with an EG&G 7220 DSP Lock-In amplifier. This monochromatic system was also used to collect all external quantum efficiency data.

Synthesis. All chemicals, reagents, and solvents were used as received from commercial sources without further purification. All glassware was oven-dried, and all reactions were performed under N_2. Compound **1** was made using the procedure described in the literature.[29]

Symmetric Squaraines, 2−8. Compounds **2**−**8** were all made by a similar synthetic procedure. The synthesis of **3** is detailed here and was followed for the preparation of the other symmetric anilino-squaraines.

Table 1. Summary of Crystal Data, Data Collection, and Refinement Parameters for 1 and 3

compound	1	3
empirical formula	$C_{32}H_{44}N_2O_6$	$C_{40}H_{28}N_2O_6$
formula weight	552.69	632.64
temperature	143(2) K	100(2) K
radiation wavelength	0.71073 Å	1.54178 Å
crystal system	monoclinic	triclinic
space group	P 2(1)/n	P-1
unit cell dimensions	a = 6.2034(16) Å	a = 11.1895(9) Å
	α = 90°	α = 96.371(8)°
	b = 16.478(4) Å	b = 11.7874(11) Å
	β = 92.406(4)°	β = 91.176(7)°
	c = 14.518(4) Å	c = 11.9792(9) Å
	γ = 90°	γ = 92.485(7)°
volume	1482.7(6) $Å^3$	1568.3(2) $Å^3$
Z	2	2
density (calculated)	1.238 Mg/m^3	1.340 Mg/m^3
absorption coefficient	0.085 mm^{-1}	0.738 mm^{-1}
F(000)	596	660
crystal size	0.33 × 0.09 × 0.05 mm^3	0.10 × 0.09 × 0.02 mm^3
theta range for data collection	1.87 to 27.52°	3.71 to 59.29°
index ranges	$-8 \le h \le 8$	$-12 \le h \le 12$
	$-21 \le k \le 20$	$-13 \le k \le 11$
	$-18 \le l \le 18$	$-13 \le l \le 13$
reflections collected	12527	14554
independent reflections	3349 [R(int) = 0.0508]	4202 [R(int) = 0.0753]
completeness to theta = 27.52°	98.4%	99.0%
absorption correction	semiempirical	multiscan
transmission factors	min/max 0.796	min/max: 0.810
refinement method	full-matrix least-squares on F^2	
data/restraints/parameters	3349/0/193	4202/6/437
goodness-of-fit on F^2	1.014	1.084
final R indices [I > 2σ(I)]	R1 = 0.0477	
wR2 = 0.1021	R1 = 0.0819	
wR2 = 0.2240		
R indices (all data)	R1 = 0.0890	
wR2 = 0.1147	R1 = 0.1154	
wR2 = 0.2434		
largest diff. peak and hole	0.218 and −0.184 e.$Å^{-3}$	0.619 and −0.322 e.$Å^{-3}$

The first synthesis given is for the preparation of N-(3,5-dihydroxyphenyl)diphenylamine, and the second the reaction of this material with squaric acid to form the N,N-diphenylanilino squaraine dye. The characterization data for **2**−**8** are given below.

N-(3,5-Dihydroxyphenyl)diphenylamine. Diphenylamine (3 g, 17.7 mmol), 1-bromo-3,5-dimethoxybenzene (4.6 g, 21 mmol), $Pd_2(dba)_3$ [tris(dibenzylidineacetone)dipalladium(0)] (0.78 g, 0.8 mmol), sodium *tert*-butoxide (2.6 g, 25 mmol), and tri-*tert*-butylphosphine (0.52 g, 2.5 mmol) were dissolved in 100 mL of toluene and refluxed under N_2 for 5 h. The reaction mixture was cooled down and passed through a plug of silica gel with toluene to remove insoluble material. The crude product was recrystallized from toluene/MeOH to obtain 4.5 g (83%) of N-(3,5-dimethoxyphenyl)diphenylamine. Next, this triarylamine (2.0 g, 6.5 mmol) was added to 70 mL of anhydrous CH_2Cl_2 in a 250 mL round-bottom flask equipped with a stir bar. Boron tribromide (65 mL of 1 M solution in CH_2Cl_2, 65 mmol) was added, and the solution was stirred under room temperature for 2 days. The solution was then decanted to 30 mL of ice water, and after 30 min of hydrolysis the organic layer was extracted twice with 100 mL of CH_2Cl_2. The organic layer was washed twice with 100 mL of cold water to neutralize any excess of BBr_3. The solvent was removed under reduced pressure, and the resulting solid was further purified on silica gel column chromatography using hexane and ethyl acetate (6:1) to obtain 1.6 g (88%) of N-(3,5-dihydroxyphenyl)diphenylamine.

3. 2-[4-(N,N-Diphenylamino)-2,6-dihydroxyphenyl]-4-[(4-(N,N-diphenyliminio)-2,6-dihydroxyphenyl)-2,5-dien-1-ylidene]-3-oxocyclobut-1-en-1-olate. A mixture of N-(3,5-dihydroxyphenyl)diphenylamine (1 g, 3.6 mmol) and excess squaric acid (0.25 g, 2.2 mmol) in 1-butanol (40 mL) and toluene (120 mL) were refluxed under N_2 overnight. After reaction was cooled down, the solvents were removed under reduced pressure using a rotary evaporator leaving behind a green solid. The crude solid was recrystallized from a 1:1 volume ratio of dichloromethane methanol mixture to afford metallic green crystals of **3** (0.70 g, 61%). ^1H NMR ($CDCl_3$, 500 MHz): 11.00 (s, 4H), 7.41

dx.doi.org/10.1021/cm2020803 |*Chem. Mater.* 2011, 23, 4789–4798

(t, 8H, J = 7.5 Hz), 7.29 (t, 4H, J = 7 Hz), 7.23 (d, 8H, J = 8 Hz), 5.87 (s, 4H). ^{13}C NMR ($CDCl_3$, 125 MHz): 181.36, 163.50, 163.06, 159.51, 144.08, 129.81, 127.57, 127.05, 104.96, 98.75. MS (ESI^+): m/z 633.3 (MH^+); calcd: 632.66 amu. Elemental analysis for $C_{40}H_{28}N_2O_6 \cdot CH_2Cl_2 \cdot MeOH$: calcd: C 74.42, H 4.42, N 4.23; found: C 74.58, H 4.31, N 4.35.

2. 2-[4-(N-Phenyl-N-methylamino)-2,6-dihydroxyphenyl]-4-[(4-(N-phenyl-N-methyliminio)-2,6-dihydroxyphenyl)-2,5-dien-1-ylidene]-3-oxocyclobut-1-en-1-olate. Yield = 17%. ^{1}H NMR ($CDCl_3$, 500 MHz, 60 °C): 10.95 (s, 4H), 7.44 (t, 4H, J = 8 Hz), 7.33 (t, 2H, J = 7.5 Hz), 7.19 (d, 4H, J = 8.5 Hz), 5.77 (s, 4H), 3.41 (s, 6H). ^{13}C NMR ($CDCl_3$, 125 MHz, 60 °C): 184.45, 163.25, 158.38, 144.08, 130.09, 127.68, 127.03, 104.96, 95.49, 86.48, 53.29. MS (ESI^+): m/z 508.25 (M^+); calcd: 508.52 amu. Elemental analysis for $C_{30}H_{24}N_2O_6 \cdot MeOH$: calcd: C 68.88, H 5.22, N 5.18; found: C 69.44, H 5.48, N 5.18.

4. 2-[4-(N-Phenyl-N-1-naphthylamino)-2,6-dihydroxyphenyl]-4-[(4-(N-phenyl-N-1-naphthyliminio)-2,6-dihydroxyphenyl)-2,5-dien-1-ylidene]-3-oxocyclobut-1-en-1-olate. Yield = 51%. ^{1}H NMR ($CDCl_3$, 500 MHz, 60 °C): 10.91 (s, 4H), 7.91 (d, 2H, J = 7.5 Hz), 7.88 (t, 4H, J = 7.5 Hz), 7.47−7.54 (m, 8H), 7.39 (d, 2H, J = 7 Hz), 7.30−7.37 (m, 8H), 7.22 (m, 4H), 5.78 (s, 4H). ^{13}C NMR ($CDCl_3$, 125 MHz, 60 °C): 181.34, 163.78, 163.24, 160.31, 144.15, 140.10, 134.99, 130.48, 129.71, 128.83, 128.69, 127.57, 127.31, 126.77, 126.74, 126.40, 126.03, 123.08, 104.87, 98.27. MS (ESI^+): m/z 733.2 (MH^+); calcd: 732.78 amu. Elemental analysis for $C_{48}H_{32}N_2O_6$: calcd: C 78.68, H 4.40, N 3.82; found: C 78.07, H 4.28, N 3.85.

5. 2-[4-(N-Phenyl-N-2-naphthylamino)-2,6-dihydroxyphenyl]-4-[(4-(N-phenyl-N-2-naphthyliminio)-2,6-dihydroxyphenyl)-2,5-dien-1-ylidene]-3-oxocyclobut-1-en-1-olate. Yield = 38%. ^{1}H NMR ($CDCl_3$, 500 MHz, 60 °C): 10.99 (s, 4H), 7.86 (d, 2H, J = 8.8 Hz), 7.82−7.86 (m, 2H), 7.73−7.77 (m, 2H), 7.66 (d, 2H, J = 2 Hz), 7.48−7.52 (m, 4H), 7.40 (t, 4H, J = 7.5 Hz), 7.32 (dd, 2H, J = 8.8, 2.1 Hz), 7.28 (t, 2H, J = 7.5 Hz), 7.27 (t, 4H, J = 7.5 Hz), 5.93 (s, 4H). ^{13}C NMR ($CDCl_3$, 125 MHz, 60 °C): 181.59, 164.10, 163.46, 159.84, 144.44, 141.78, 134.01, 132.14, 129.90, 129.86, 127.86, 127.81, 127.70, 127.12, 126.93, 126.59, 125.86, 125.58, 105.45, 99.33. MS (ESI^+): m/z 733.3 (MH^+); calcd: 732.78 amu. Elemental analysis for $C_{48}H_{32}N_2O_6$: calcd: C 78.68, H 4.40, N 3.82; found: C 78.74, H 4.33, N 3.84.

6. 2-[4-(N,N-4,4′-Biphenylamino)-2,6-dihydroxyphenyl]-4-[(4-(N,N-4,4′-biphenyliminio)-2,6-dihydroxyphenyl)-2,5-dien-1-ylidene]-3-oxocyclobut-1-en-1-olate. Yield = 28%. ^{1}H NMR ($CDCl_3$, 500 MHz, 60 °C): 11.00 (s, 4H), 7.63 (d, 8H, J = 8.5 Hz), 7.60 (d, 8H, J = 7.8 Hz), 7.45 (t, 8H, J = 7.4 Hz), 7.36 (t, 4H, J = 7.4 Hz), 7.31 (d, 8H, J = 8.5 Hz), 6.00 (s, 4H). The solubility of **6** was too poor to obtain an acceptable ^{13}C NMR spectrum. Elemental analysis for $C_{64}H_{44}N_2O_6$: calcd: C 82.03, H 4.73, N 2.99; found: C 83.9, H 4.31, N 1.75.

7. 2-[4-(N,N-2,2′-Biphenylamino)-2,6-dihydroxyphenyl]-4-[(4-(N,N-2,2′-biphenyliminio)-2,6-dihydroxyphenyl)-2,5-dien-1-ylidene]-3-oxocyclobut-1-en-1-olate. Yield = 19%. ^{1}H NMR ($CDCl_3$, 500 MHz, 60 °C): 11.00 (s, 4H), 7.24 (m, 4H), 7.22 (t, 8H, J = 7.5 Hz), 7.08−7.14 (m, 8H), 6.97 (d, 8H, J = 7.1 Hz), 6.82 (t, 4H, J = 7.1 Hz), 6.27 (d, 4H, J = 7.8 Hz), 5.89 (s, 4H). ^{13}C NMR ($CDCl_3$, 125 MHz, 60 °C): 181.44, 163.11, 163.06, 140.26, 140.15, 139.62, 131.43, 129.91, 128.55, 128.25, 127.38, 127.27, 127.02, 104.76, 98.00. MS (ESI^+): m/z 937.4 (MH^+); calcd: 937.04 amu. Elemental analysis for $C_{64}H_{44}N_2O_6$: calcd: C 82.03, H 4.73, N 2.99; found: C 81.98, H 4.70, N 3.02.

8. 2-[4-(N-Phenyl-N-1-pyrenylamino)-2,6-dihydroxyphenyl]-4-[(4-(N-phenyl-N-1-pyrenyliminio)-2,6-dihydroxyphenyl)-2,5-dien-1-ylidene]-3-oxocyclobut-1-en-1-olate. Yield = 60%. ^{1}H NMR ($CDCl_3$, 500 MHz, 60 °C): 10.89 (s, 4H), 8.24 (d, 2H, J = 7.5 Hz), 8.20 (d, 2H, J = 7.4 Hz), 8.19 (d, 2H, J = 8.2 Hz), 8.02−8.15 (m, 10H), 7.85 (d, 2H, J = 8.1 Hz), 7.32−7.39 (m, 4H), 7.20−7.24 (m, 2H), 5.81 (s, 4H). ^{13}C NMR ($CDCl_3$, 125 MHz, 60 °C): 181.52, 164.17, 163.63, 160.78, 144.70, 137.32, 131.29, 131.01, 129.79, 129.44, 128.39, 127.07, 126.99, 126.71, 126.62, 126.09, 125.88, 125.84, 124.73, 122.07, 105.28, 98.79. MS (ESI^+): m/z 881.5 (M^+); calcd: 884.97 amu. Elemental analysis for $C_{60}H_{40}N_2O_6 \cdot CH_2Cl_2 \cdot MeOH$: calcd: C 80.16, H 4.52, N 3.06; found: C 80.10, H 3.81, N 3.11.

Unsymmetrical Squaraines, 9 and 10. The synthesis of **9** and **10** were carried out by similar procedures. The first step involved the synthesis of diphenylaminosquarate, followed its reaction with either N-(3,5-dihydroxyphenyl)diisobutylamine or N-(3,5-dihydroxyphenyl)-diphenylamine to give **9** or **10**.

3-Diphenylamino-4-hydroxycyclobut-3-ene-1,2-dione (diphenylaminosquarate).[30] A solution of diphenylamine (5.0 g, 30 mmol) in 100 mL of propan-2-ol was added to a solution of 3,4-diisopropoxycyclobut-3-ene-1,2-dione (4.7 g, 24 mmol) in 50 mL of the same solvent. Concentrated HCl (1 mL) was then added, and the mixture was refluxed for approximately 3 h. The solvent was removed on a rotary evaporator, and the residue was dissolved in $CHCl_3$ and filtered to remove any squaric acid. The filtrate was then pumped down, and the residue was dissolved in 150 mL of acetone and followed by 150 mL of 6 M HCl. This solution was refluxed for 4 h with vigorous stirring followed by evaporation under reduced pressure to give a residue that was subsequently dissolved in $CHCl_3$ and filtered to remove any further quantities of residual squaric acid. The solvent was removed from the filtrate under reduced pressure, and the residue repeatedly was extracted with hot water to give green crystals of the product. This material was recrystallized once more from hot water to obtain 3.7 g (59%) of diphenylaminosquarate. ^{1}H NMR ($CDCl_3$, 500 MHz, 60 °C): 7.41 (t, 2H, J = 7.5 Hz), 7.35 (t, 1H, J = 7.5 Hz), 7.16 (d, 2H, J = 7.5 Hz), 5.61 (s, 1H), 3.41(s, 3H). ^{13}C NMR ($CDCl_3$, 125 MHz, 60 °C): 181.36, 163.06, 159.51, 144.08, 129.81, 127.57, 104.96, 98.75.

9. 2-[4-(N,N-Diisobutylamino)-2,6-dihydroxyphenyl]-4-(4-diphenyliminio)-2,5-dien-1-ylidene}-3-oxocyclobut-1-en-1-olate. A solution of diphenylaminosquarate (1.5 g, 5.7 mmol) and N-(3,5-dihydroxyphenyl) diisobutylamine (1.35 g, 5.7 mmol) in 45 mL of toluene and 15 mL of 1-butanol was refluxed under N_2 overnight. The resulting reaction mixture was dried over rotary evaporator to obtain a crude red solid. The final product was purified by elution with CH_2Cl_2/hexane on a silica gel column to obtain 0.76 g (28%) of **9**. ^{1}H NMR ($CDCl_3$, 500 MHz, 60 °C): 12.00 (s, 2H), 7.43−7.47 (m, 4H), 7.36−7.39 (m, 2H), 7.21−7.23 (m, 4H), 5.76 (s, 2H), 3.21 (d, 4H, J = 7.5 Hz), 2.12 (sep, 2H, J = 6.7 Hz), 0.90 (d, 12H, J = 6.7 Hz). ^{13}C NMR ($CDCl_3$, 125 MHz, 60 °C): 175.59, 163.59, 139.98, 129.17, 128.07, 125.31, 93.82, 60.25, 27.56, 20.16. MS (ESI^+): m/z 485.4 (MH^+); calcd: 484.58 amu. Elemental analysis for $C_{30}H_{32}N_2O_4$: calcd: C 74.36, H 6.66, N 7.78; found: C 74.33, H 6.75, N 5.80.

10. 2-[4-(N,N-Diphenylamino)-2,6-dihydroxyphenyl]-4-(4-diphenyliminio)-2,5-dien-1-ylidene}-3-oxocyclobut-1-en-1-olate. A solution of diphenylaminosquarate (0.5 g, 1.9 mmol) and N-(3,5-dihydroxyphenyl)diphenylamine (0.56 g, 2.0 mmol) in 45 mL of toluene and 15 mL of 1-butanol was refluxed under N_2 overnight. The resulting reaction mixture was dried under reduced pressure in a rotary evaporator to obtain a crude red solid. The final product was purified by elution with CH_2Cl_2/hexane on a silica gel column to obtain 0.12 g (11%) of **10**. ^{1}H NMR ($CDCl_3$, 500 MHz, 60 °C): 11.88 (s, 2H), 7.48−7.51 (m, 4H), 7.42−7.46 (m, 2H), 7.35−7.39 (m, 4H), 7.26 (m, 2H), 7.24−7.26 (m, 4H), 7.21−7.23 (m, 4H), 5.84 (s, 2H). ^{13}C NMR ($CDCl_3$, 125 MHz, 60 °C): 175.34, 163.41, 144.36, 139.50, 129.56, 129.12, 128.51, 127.50, 126.42, 125.28, 99.14. MS (ESI^+): m/z 525.35 (MH^+); calcd: 524.56 amu. Elemental analysis for $C_{34}H_{24}N_2O_4 \cdot CH_2Cl_2$: calcd: C 76.27, H 5.19, N 4.81; found: C 76.35, H 4.49, N 5.28.

RESULTS AND DISCUSSION

Synthesis. The synthesis of bis(N,N-*alkyl*anilino)squaraines is typically accomplished by the reaction between squaric acid

Scheme 1

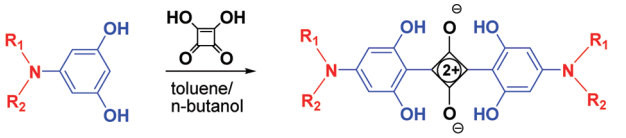

1. $R_1 = R_2$ = isobutyl
2. R_1 = methyl, R_2 = phenyl
3. $R_1 = R_2$ = phenyl
4. R_1 = 1-naphthyl, R_2 = phenyl
5. R_1 = 2-naphthyl, R_2 = phenyl
6. $R_1 = R_2$ = 4-biphenyl
7. $R_1 = R_2$ = 2-biphenyl
8. R_1 = 1-pyrenyl, R_2 = phenyl

and an N,N-dialkylaniline.[29,31,32] However, a synthesis using an amine that has two different N-aryl groups, necessary for the formation of N,N-di*aryl*anilino squaraines, may encounter problems with respect to the selectivity of electrophilic substitution.[33] To eliminate this possibility, we chose to substitute one aryl ring with two activating *meta*-hydroxyl groups in order to direct electrophilic attack by the squarate ion on this ring. The presence of hydroxyl groups can also serve to impart higher thermal stability and structural rigidity to the resultant squaraines.[29]

The N,N-diarylamines needed for the preparation of the squaraines were obtained from commercial sources or synthesized from aniline and aryl bromides using Buchwald-Hartwig amination.[34−36] N-(3,5-Dimethoxyphenyl)-N,N-diarylamines in turn were prepared in yields up to 90% using a Buchwald-Hartwig reaction between 1-bromo-3,5-dimethoxybenzene and the appropriate diarylamines (see the Supporting Information). The methoxy groups of these triarylamines were then deprotected using BBr_3 in CH_2Cl_2.[37] Symmetric squaraines **2**−**8** were obtained in yields up to 60% by refluxing two equivalents of the corresponding amine and one equivalent of squaric acid in a mixture of 1-butanol and toluene for 10 h (Scheme 1). The isolation of the squaraines was carried out by simple crystallization methods which allowed us to obtain high purity samples in gram quantities. The composition of **2**−**8** was confirmed using standard characterization methods: ^{1}H NMR, ^{13}C NMR spectroscopy, and elemental analyses. Thermal gravimetric analysis (TGA) was performed on squaraines **1**, **3**, and **4** to assess if thermal stability was improved by the N-aryl substituents. The squaraines were found to undergo 5% weight loss at 308 °C (**1**), 318 °C (**3**), and 326 °C (**4**). The modest increase in decomposition temperature for the N-aryl derivatives suggests that the thermal breakdown occurs at the squarate moiety. Consequently, attempts to sublime samples of **3** and **4** led to extensive decomposition.

Single crystal X-ray structures were obtained for crystals of **1** obtained from CH_2Cl_2/MeOH and **3** obtained from toluene (Figure 1). The metrical parameters of both derivatives are similar to values reported for related bis[N,N-di(n-butyl)anilino]-squaraines.[38,39] A relatively short aryl−squarate bond distance (C2−C3 = 1.402(2) Å in **1**, C16−C19 = 1.409(7) Å in **3**) is consistent with strong conjugation between the anilino moieties and squarate core. Likewise, the short nitrogen−anilino bond distances (N1−C6 = 1.359(2) Å in **1**, N1−C13 = 1.385(6) Å in **3**) demonstrate strong conjugative stabilization imparted by the amino substituent to the squaraine, particularly when compared to the considerably longer nitrogen −phenyl bonds in **3** (average = 1.435(6) Å). The average hydroxy−squarate oxygen O−H···O bond distances (O···O = 2.651 Å in **1** and 2.652 Å in **3**) are within values previously assigned to intramolecular hydrogen bonds in related squaraines.[40]

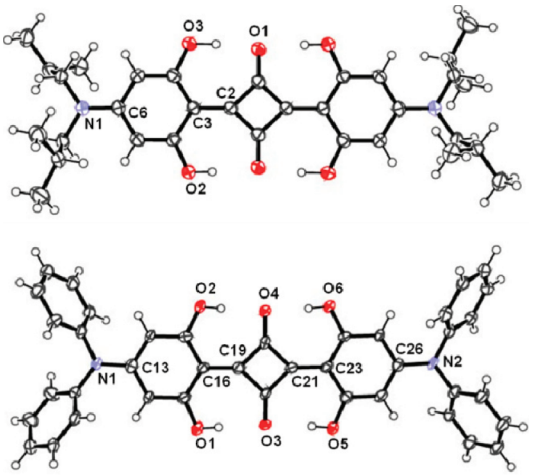

Figure 1. ORTEP diagrams for **1** (top) and **3** (bottom).

The π-system of **1** is nearly planar as there is only a small dihedral twist (<4 degrees) between the dihydroxy-phenyl ring and squarate core, whereas **3** displays a slightly twisted conformation with dihedral angles of ca. 10° and 13° between the dihydroxy-phenyl rings and squarate core. The amine groups of **1** and **3** are planar; the sum of the three C−N−C bond angles for the amine groups of both **1** and **3** are 360°. The amine groups of **3** show larger dihedral twists with respect to the dihydroxyphenyl group (12.2° and 13.2°) as compared to the corresponding dihedral angles for the amine groups of **1** (0.95°).

Packing diagrams of **1** and **3** show significant differences in the organization of squaraine molecules in the crystal lattice (Figure 2). Squaraine molecules in crystals of **1** are organized in staircase slip-stacked columns arranged in herringbone-like arrays that alternate at skewed 90° angles with respect to the molecular long axis (Figure 2a). To describe the angular inclinations away from the molecular plane within the stacks, it is instructive to use "pitch" and "roll" angles, terms coined by Curtis et al.[41] The pitch angle defines the displacement with respect to the long molecular axis, while the roll angle identifies the displacement relative to the short molecular axis. The squaraine planes are separated by ca. 3.2 Å and have pitch and roll angles of 45° and 36°, respectively. The small roll angle in particular leads to a displacement along the short axis by more than 3 Å such that there is no π-overlap between aromatic rings in adjacent molecules (Figure 2b). In contrast, crystals of **3** are composed of dimers separated by ca. 3.4−3.5 Å between the molecular planes arranged in parallel columns. The columns of **3** are also organized in a slip-stack staircase arrangement with the long molecular axis having a pitch angle of ca. 38° (Figure 2c). However, unlike **1**, a large roll angle of 80° within the stack leads to a small displacement along the short molecular axis (Figure 2d). While there are no significant π-interactions between the pendant phenyl rings of adjacent squaraine molecules, the small lateral displacement leads to considerable π-overlap between the anilinosquaraine ring systems within the stack. The small pitch angle leads to a large slip offset in the long molecular axis such that the squarate core is situated above the aromatic anilino ring in adjacent molecules. Molecular solids with large roll angles and slip offsets, and consequent cofacial π-stacking as found in crystals of **3**, have been proposed to have better charge and exciton transport properties in ordered films than materials with small roll angles and poor π-overlap, as observed in **1**.[41]

dx.doi.org/10.1021/cm2020803 |*Chem. Mater.* 2011, 23, 4789–4798

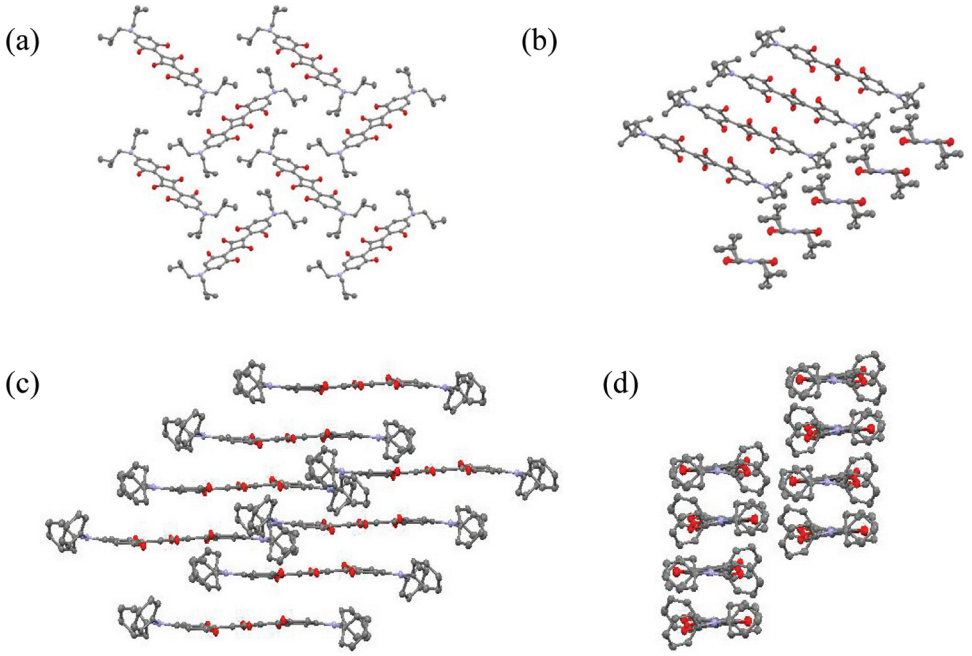

Figure 2. Crystal packing diagrams for **1** (top) and **3** (bottom). View of **1** showing herringbone structure (a) and molecular stacking arrangement (b). Stacking arrangement of **3** viewed down the short (c) and long (d) molecular axes. Hydrogen atoms were removed for clarity.

Scheme 2

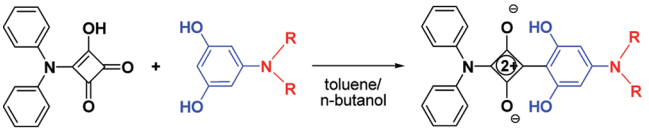

9. R = isobutyl **10**. R = phenyl

Good solubility is essential to prepare smooth, uniform films in OPVs.[42] Typically, bis(N,N-di*alkyl*anilino)squaraines have poor solubility unless modified with bulky substituents such as the isobutyl groups in **1**. Similarly, the squaraine with N-methyl-N-phenyl groups (**2**) has poor solubility. In contrast, most of the bis(N,N-di*aryl*anilino)squaraines, in particular **3** and **4**, are soluble in common organic solvents such as toluene, dichloromethane, chlorobenzene, *etc.* and form pinhole-free film upon spin-casting. Interestingly, the site of aryl substitution also affects the solubility of bis(N,N-di*aryl*anilino) squaraines. For example, the derivative with N,N-(1-naphthyl)phenyl substituents (**4**) has one of the highest solubilities in the studied series, whereas the isomeric squaraine with N,N-(2-naphthyl)phenyl substituents (**5**) is only moderately soluble (<1 mg/mL in CH_2Cl_2). Likewise, squaraine **7**, which has ortho N,N-2-biphenyl substituents, is more soluble than the para N,N-4-biphenyl analog **6**.

While squaraines **1**−**8** absorb in the red, derivatives that absorb shorter wavelengths are also desired to achieve improved overlap with the solar spectrum. Decreasing the extent of π-conjugation in aromatic dye systems typically causes a hypsochromic shift in absorption and, to that end, unsymmetrical squaraines having only one anilino group bound to the squarate core were prepared (Scheme 2). Addition of one equivalent of diphenylamine to diisopropoxysquarate, followed by acid hydrolysis, forms a monoamino squarate adduct that has a second squaric acid site available for further functionalization.[30,43] Subsequent reaction between the monoamino squarate and either N-(3,5-dihydroxyphenyl)diisobutylamine or N-(3,5-dihydroxyphenyl)diphenylamine forms the corresponding squaraines **9** and **10** in low to moderate yields. The reaction is complicated by partial decomposition of the mono adduct to reform squaric acid and diphenylamine, leading to the formation of the corresponding symmetrical squaraines **1** or **3** as impurities. However, **1** and **3** can be readily removed by fractional crystallization or column chromatography, giving pure samples of **9** and **10**, respectively. Like squaraines **3** and **4**, compounds **9** and **10** are soluble in organic solvents (>5 mg/mL) and form high quality films when spun cast from solution.

Photophysical and Electrochemical Characterization. The absorption properties of squaraines **1**−**10** in CH_2Cl_2 solution and in neat thin film are listed in Table 2, and representative spectra are shown for **1**, **3**, and **10** in Figure 3a. In solution, squaraines **1**−**8** display an intense ($\varepsilon \approx 10^5$ M^{-1} cm^{-1}) absorption band with λ_{max} = 650−700 nm. Relative to the absorption maximum of **1** (λ_{max} = 645 nm) and other N,N-dialkyl derivatives,[44] N-aryl squaraines **2**−**8** show red-shifted peak maxima, Table 1. In contrast, the unsymmetrical squaraines **9** and **10** have absorption peaks that are blue-shifted ($\lambda_{max} \sim$ 530 nm) relative to both N-*alkyl*anilino and N-*aryl*anilino based symmetric squaraines. The absorption bands of **1** and **2** in solution display narrow full-width half maxima (fwhm) of 630 cm^{-1} and 890 cm^{-1}, respectively, while the absorption bands of **3**−**10** are markedly broader, with fwhm between 1280 and 1980 cm^{-1}. The absorption spectra for all the squaraines red-shift and undergo significant broadening in thin films (Figure 3a). The broadening is important for OPVs since it leads to improved spectral overlap with the solar irradiance spectrum.

Squaraines **1**−**10** fluoresce in the wavelength range of λ_{max} = 658−758 nm (Table 2), and representative excitation and emission spectra for **1** and **3** are shown in Figure 3b. The excitation

dx.doi.org/10.1021/cm2020803 |*Chem. Mater.* 2011, 23, 4789–4798

Table 2. Photophysical Data for Squaraines 1−10 in Solution and As Thin Films

	absorption					emission	
	solution in CH_2Cl_2 or (toluene)			thin film		toluene solution	
	ε (10^5 M^{-1} cm^{-1})	λ_{max} (nm)	fwhm (cm^{-1})	λ_{max} (nm)	fwhm (cm^{-1})	λ_{em} (nm)	Φ
1	4.1	652 (649)	630	692	3140	658	0.80
2	1.7	645 (645)	890	*a*	*a*	672	0.14
3	1.9	674 (677)	1470	717	3240	750	0.29
4	2.0	666 (669)	1280	691	3280	726	0.36
5	1.9	687 (689)	1590	717	2770	768	0.07
6	0.71	694 (693)	1790	697	2910	786	0.02
7	2.1	678 (673)	1440	686	2490	721	0.66
8	1.4	679 (682)	1530	712	2520	738	0.02
9	1.3	529 (529)	1570	552	2840	582	0.01
10	1.0	535 (539)	1980	560	3160	625	0.02

[a] Solubility is too poor to form a uniform film.

spectra of **1**−**10** match the absorption profiles, although structure seen in the excitation spectrum of **3** suggests small variations in the luminescent response from conformational isomers. The photoluminescent quantum efficiency (Φ) of **1** in toluene is 0.80, whereas **2**−**10** are lower, ranging from 0.01 to 0.66. The Stokes shift of the N-*alkyl*anilino-squaraine **1** is 9 nm in toluene and is unaffected by solvents of higher polarity. The small, solvent-insensitive Stokes shift is comparable to behavior observed for other related N,N-di*alkyl*anilino squaraines[44,45] indicating that only minor structural reorganization occurs in the excited state.[46] On the other hand, the N-*aryl*anilinosquaraines display much larger Stokes shifts that range between 27 nm for **2** to 79 nm for **5**. The large Stokes shifts observed for **2**−**10** suggests that excited state formation in the N-*aryl*anilino derivatives is accompanied by a greater degree of intramolecular distortion than occurs in **1**.[47] In addition, the Stokes shift increases with increasing solvent polarity (positive solvatochromism). For example, the Stokes shift of **3** is 52 nm in cyclohexane, 73 nm in toluene, and 112 nm in 2-methyltetrahydrofuran (2MeTHF). The solvatochromic response indicates that the excited state of **3** is both more polarizable than that of **1** and strongly stabilized by polar media.

The solvent-dependent luminescence properties of squaraines **1** and **3** were examined in more detail. The quantum yield of **1** is largely independent of solvent polarity, ranging from 0.80 in toluene to 0.73 in acetonitrile. This behavior differs from the trend reported for bis[4-(N,N-dimethyl)anilino]squaraine (SQ-DMA),[48] an analogue of **1** without the *meta*-hydroxyl groups. The quantum yield of SQ-DMA is also high in toluene (Φ = 0.85) but decreases dramatically in acetonitrile (Φ = 0.08). The lower quantum yield of SQ-DMA in polar media was attributed to the formation of a twisted intramolecular charge transfer (TICT) state that acts as a nonradiative decay channel.[48,49] Rotation around the N,N-dimethylanilino−squarate bond axis was proposed to accompany formation of the TICT state. The weak solvent dependence in the quantum yield of **1** suggests that an analogous TICT state is not accessible in this compound. The difference between **1** and SQ-DMA likely arises due to hydrogen bonds formed between the four hydroxyl groups to the squarate oxygens in **1** that suppress twisting along the phenyl−squarate bond. Like SQ-DMA, the quantum yield of **3** is strongly affected by solvent polarity, being highest in cyclohexane (Φ = 0.55) and decreasing sharply in 2-MeTHF (Φ = 0.05). This suggests that an alternate TICT state may be accessible in **3**. Since both squaraine **1** and **3** have equivalent hydroxyl groups, twisting of the diphenylamino moiety with respect to the molecular core might account for the dependence of quantum yield on the solvent polarity. Considering that the dipolar structure of **3** should lead to a nominally nonpolar ground state, the luminescent quenching behavior implies that charge separation, along with consequent breaking of the molecular symmetry, occurs during formation of the TICT excited state.

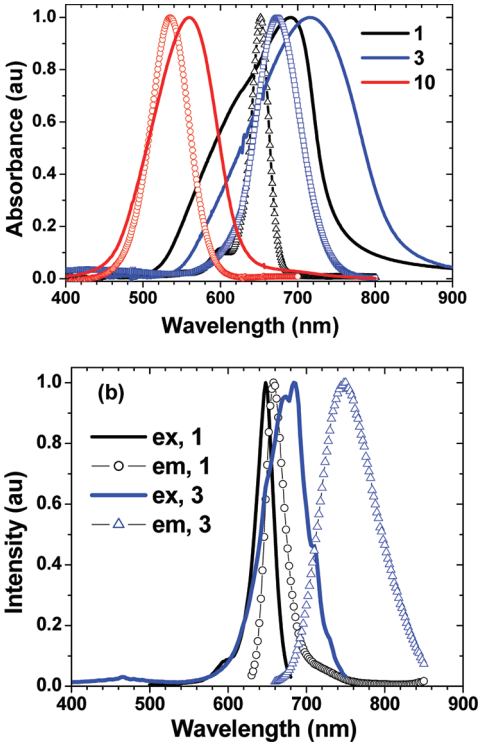

Figure 3. (a) Absorption spectra for **1**, **3**, and **10** in CH_2Cl_2 solution (open symbols) and as neat films (solid lines). (b) Excitation (ex) and emission (em) spectra of **1** and **3** in toluene.

dx.doi.org/10.1021/cm2020803 |*Chem. Mater.* 2011, 23, 4789–4798

Table 3. Electrochemical Redox Potentials[a] and Calculated HOMO/LUMO Energies[b] for Squaraines 1−10 along with HOMO Energies from UPS Measurements for 1, 2−5, and 10

squaraines	E_{ox} (V)	E_{red} (V)	HOMO (eV)[c]	LUMO (eV)
1	0.49, r	−1.23, i	5.29 (5.1)	3.31
2	0.54, q	−1.25, i	5.36	3.29
3	0.62, r	−1.08, i	5.47 (5.3)	3.49
4	0.59, q	−1.24, i	5.43(5.3)	3.30
5	0.58, r	−1.11, i	5.41 (5.3)	3.45
6	0.59, q	−1.12, i	5.43	3.45
7	0.60, r	−1.10, r	5.44	3.47
8	0.65, q	−0.98, q	5.51	3.61
9	0.59, r	−1.40, r	5.43	3.11
10	0.70, r	−1.45, i	5.58 (5.4)	3.05

[a] Recorded in 0.1 M $Bu_4N^+PF_6^-$ in CH_2Cl_2, referenced to internal Fc^+/Fc; r = reversible, q = quasi-reversible, and i = irreversible. Values for irreversible waves are cathodic peak potentials. [b] HOMO[50] and LUMO[51] values calculated from redox data using methods described in the literature. [c] HOMO values from UPS measurements are given in parentheses.

Electrochemical analysis of **1**−**10** using both cyclic and differential pulse voltammetry were performed in CH_2Cl_2 and referenced to Fc^+/Fc as an internal standard, and redox data are listed in Table 3. Squaraines **1**−**8** display reversible or quasi-reversible oxidation waves in the range 0.49−0.65 V and irreversible reduction waves between −0.98 V and −1.25 V. Compared to squaraine **1** (E_{ox} = 0.49 V), the oxidation potentials of **2**−**8** are 0.05 to 0.16 V lower. Unsymmetrical squaraines **9** and **10** show reversible oxidation at comparable potentials (E_{ox} = 0.59 and 0.70 V, respectively) but display reversible reduction at higher potentials (E_{red} = −1.40 V and −1.45 V, respectively), which indicate that the blue shift in absorption is primarily due to an increase in the energy of the LUMO. The energy of the HOMO for films of **1**, **3**, **4**, **5**, and **10** has also been determined using ultraviolet photoelectron spectroscopy (UPS). The first ionization potential of squaraine **3**, **4**, and **5** are the same (IP_1 = 5.3 eV) and 0.2 V higher than **1** (IP_1 = 5.1 eV),[21] while squaraine **10** has an ionization energy of 5.4 eV.

Photovoltaic Cell Properties. The electrochemical and UPS data suggest that the N-aryl squaraines can serve as efficient donor materials when paired with C_{60} as an acceptor in OPVs. Thus, solar cells with the structure ITO/squaraine (66−85 Å)/C_{60}(400 Å)/BCP(100 Å)/Al(1000 Å) were fabricated using **1**, **3**, **4**, and **5** to study the effects of N-aryl substitution on the optoelectronic characteristics of OPVs. The performance of these devices using layers of the squaraines spun cast from chloroform is shown in Figure 4a. Current−density versus voltage (J−V) characteristics were measured in the dark and under simulated one sun (1 kW/m^2) AM1.5G illumination. The power conversion efficiencies of squaraines **3** (η = 3.2 ± 0.1%) and **4** (η = 2.5 ± 0.1%) were significantly higher than that of **1** (η = 1.8 ± 0.1%). Figure 4b clearly shows response from the squaraines (550−850 nm), along with that from C_{60} (400−550 nm), in good agreement with the absorption spectra. The V_{oc} for devices made using **3** and **4** are also 0.23 V higher than that of **1**, consistent with the decrease of the HOMO energy by 0.2 V. Further, devices made using **3** have an increased short circuit current−density (J_{sc} = 6.71 ± 0.1 mA/cm^2). An increase in fill factor (*FF*) from 0.51 ± 0.3 for **1** to near 0.60 for **3** and **4** is consistent with improved charge carrier transport for the latter

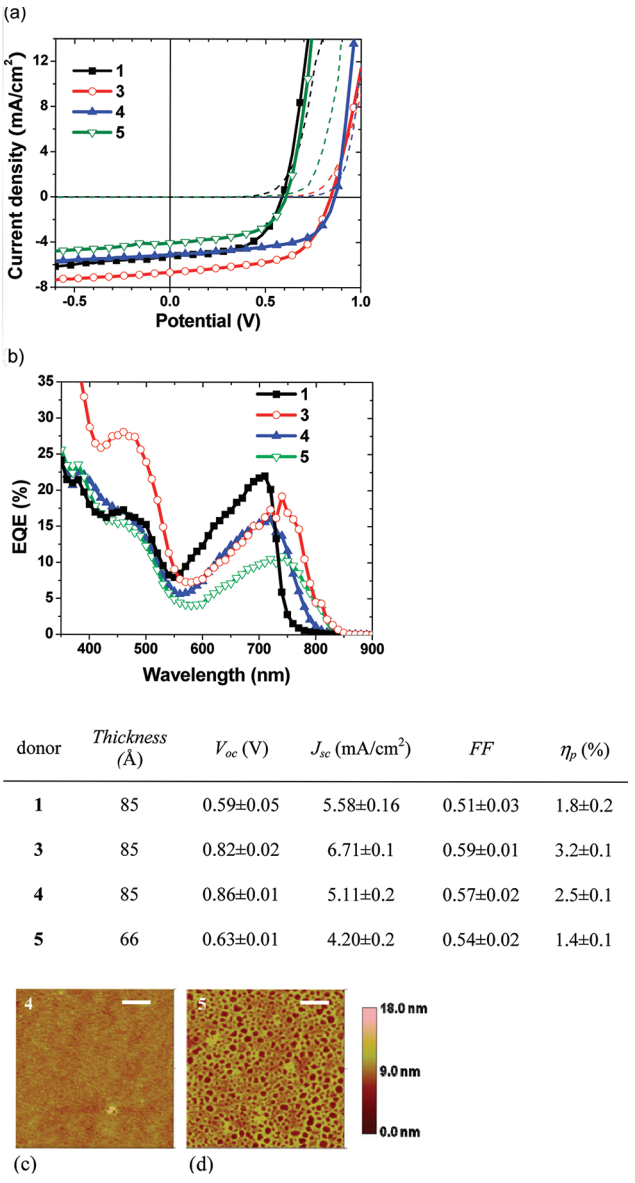

donor	*Thickness* (Å)	V_{oc} (V)	J_{sc} (mA/cm^2)	*FF*	η_p (%)
1	85	0.59±0.05	5.58±0.16	0.51±0.03	1.8±0.2
3	85	0.82±0.02	6.71±0.1	0.59±0.01	3.2±0.1
4	85	0.86±0.01	5.11±0.2	0.57±0.02	2.5±0.1
5	66	0.63±0.01	4.20±0.2	0.54±0.02	1.4±0.1

Figure 4. (a) Potential−current density and (b) external quantum efficiency (EQE) plots, along with tabulated OPV performance characteristics of squaraine donor devices with the structure ITO/squaraine (66−85 Å)/C_{60} (400 Å)/BCP (100 Å)/Al. (c) AFM images of films of **4** (rms = 0.51 nm) and (d) **5** (rms = 1.61 nm) spin-cast from chloroform. The scale bar in the top right corner is 1 μm.

materials. The role of the N-aryl substituent position is illustrated by comparing the performance of solar cells fabricated using isomeric squaraines **4** and **5**. The device made using **5** has a lower V_{oc} and J_{sc} that cannot be explained solely on the basis of differing photophysical and electrochemical characteristics of the two donor molecules. Atomic force microscopy (AFM) images show that amorphous films of **4** (Figure 4c) are smooth (rms = 0.51 nm), whereas films cast from the less soluble **5** (Figure 4d) are rough (rms = 1.61 nm). The AFM data suggest that the aromatic substituents in isomeric squaraines **4** and **5** strongly influence the molecular packing and aggregation in the films. Thus, the performance of OPVs made using **4** and **5** show a strong correlation with the differences in squaraine solubility. While the OPV efficiencies reported here are encouraging, higher

dx.doi.org/10.1021/cm2020803 |*Chem. Mater.* 2011, 23, 4789–4798

efficiencies can be achieved by thermally annealing the squaraine film and adding a buffer layer, resulting in an efficiency >5%.[52]

SUMMARY

New derivatives of symmetric bis(N,N-diaryl)anilinosquaraine dyes has been prepared using a facile and readily scalable synthesis. Unsymmetrical mono(N,N-di*aryl*anilino)squaraines are also reported. The absorption spectra of the mono- and bis(N,N-di*aryl*anilino)squaraines, which span the green, red, and near-infrared spectral regions, provide substantial overlap with the solar spectrum. The nature of the N-aryl ring strongly affects the solubility of the squaraines and consequently, the morphology of solution cast thin films. The N-aryl groups lower the HOMO energy levels relative to squaraines with N-alkyl groups; thus OPVs incorporating bis(N-di*aryl*anilino)squaraines as a donor material show a significant increase in open-circuit voltage as well as improved charge carrier transport compared to their unsubstituted analogs. Previously, we have found that thermal and solvent annealing of films of **1** can lead to significantly enhanced OPV performance.[20,22] We are currently exploring these approaches to improve the OPV performance of devices using bis(N,N-di*aryl*anilino)squaraines as well as preparing other N-aryl derivatives with enhanced optoelectronic properties. The ability to tailor the molecular and solid state optoelectronic properties of anilinosquaraines with N-aryl substituents opens up a new avenue for exploration to exploit the unique characteristics of these materials.

ASSOCIATED CONTENT

Supporting Information. Synthesis and characterization data for N-(3,5-dihydroxyphenyl)-N,N-diarylamines, ^{1}H- and ^{13}C NMR spectra for **2**−**10**, thermogravimetric traces for **1**, **3**, and **4**, absorption spectra in CH_2Cl_2 and thin films for squaraines **1**−**10** reported here (only those for **1**, **3**, and **10** are given in the text), electrochemical data for **1**−**10**, and crystallographic details for compounds **1** and **3** are given. This material is available free of charge via the Internet at http://pubs.acs.org.

AUTHOR INFORMATION

Corresponding Author
*E-mail: met@usc.edu.

ACKNOWLEDGMENT

Funding for this research was provided by the Center for Advanced Molecular Photovoltaics (CAMP) (award KUS-C1-015-21) of the King Abdullah University of Science and Technology (KAUST), the US Department of Energy Frontier Center at the University of Southern California (award DE-SC0001011, S.W. and M.E.T.), the US Department of Energy EERE Beyond the Horizon program (DE-FG36-08GO18022, G. W. and S.R.F.), and the Global Photonic Corporation. We also like to thank Dr. Frederico A. Rabuffetti for assistance with the TGA measurements.

REFERENCES

(1) Beverina, L.; Salice, P. *Eur. J. Org. Chem.* **2010**, *2010*, 1207–1225.
(2) Sreejith, S.; Carol, P.; Chithra, P.; Ajayaghosh, A. *J. Mater. Chem.* **2008**, *18*, 264–274.
(3) Tam, A. C. *Appl. Phys. Lett.* **1980**, *37*, 978–981.
(4) Law, K. Y. *J. Imaging Sci.* **1987**, *31*, 83–93.
(5) Law, K. Y. *Chem. Rev.* **1993**, *93*, 449–486.
(6) Jipson, V. B.; Jones, C. R. *J. Vac. Sci. Technol.* **1981**, *18*, 105–109.
(7) Prabhakar, C.; Bhanuprakash, K.; Rao, V. J.; Balamuralikrishna, M.; Rao, D. N. *J. Phys. Chem. C* **2010**, *114*, 6077–6089.
(8) Beverina, L.; Crippa, M.; Landenna, M.; Ruffo, R.; Salice, P.; Silvestri, F.; Versari, S.; Villa, A.; Ciaffoni, L.; Collini, E.; Ferrante, C.; Bradamante, S.; Mari, C. M.; Bozio, R.; Pagani, G. A. *J. Am. Chem. Soc.* **2008**, *130*, 1894–1902.
(9) Quartarolo, A. D.; Sicilia, E.; Russo, N. *J. Chem. Theory Comput.* **2009**, *5*, 1849–1857.
(10) Lee, Y. D.; Lim, C. K.; Kim, S.; Kwon, I. C.; Kim, J. *Adv. Funct. Mater.* **2010**, *20*, 2786–2793.
(11) Merritt, V. Y.; Hovel, H. J. *Appl. Phys. Lett.* **1976**, *29*, 414–415.
(12) Silvestri, F.; Irwin, M. D.; Beverina, L.; Facchetti, A.; Pagani, G. A.; Marks, T. J. *J. Am. Chem. Soc.* **2008**, *130*, 17640–17641.
(13) Silvestri, F.; Lopez-Duarte, I.; Seitz, W.; Beverina, L.; Martinez-Diaz, M. V.; Marks, T. J.; Guldi, D. M.; Pagani, G. A.; Torres, T. *Chem. Commun.* **2009**, 4500–4502.
(14) Bagnis, D.; Beverina, L.; Huang, H.; Silvestri, F.; Yao, Y.; Yan, H.; Pagani, G. A.; Marks, T. J.; Facchetti, A. *J. Am. Chem. Soc.* **2010**, *132*, 4074–4075.
(15) Mayerhoffer, U.; Deing, K.; Gruss, K.; Braunschweig, H.; Meerholz, K.; Wurthner, F. *Angew. Chem., Int. Ed.* **2009**, *48*, 8776–8779.
(16) Volker, S. F.; Uemura, S.; Limpinsel, M.; Mingebach, M.; Deibel, C.; Dyakonov, V.; Lambert, C. *Macromol. Chem. Phys.* **2010**, *211*, 1098–1108.
(17) Geiger, T.; Kuster, S.; Yum, J. H.; Moon, S. J.; Nazeeruddin, M. K.; Gratzel, M.; Nuesch, F. *Adv. Funct. Mater.* **2009**, *19*, 2720–2727.
(18) Yum, J. H.; Walter, P.; Huber, S.; Rentsch, D.; Geiger, T.; Nuesch, F.; De Angelis, F.; Gratzel, M.; Nazeeruddin, M. K. *J. Am. Chem. Soc.* **2007**, *129*, 10320–10321.
(19) Wang, S. Y.; Mayo, E. I.; Perez, M. D.; Griffe, L.; Wei, G. D.; Djurovich, P. I.; Forrest, S. R.; Thompson, M. E. *Appl. Phys. Lett.* **2009**, 94.
(20) Wei, G. D.; Lunt, R. R.; Sun, K.; Wang, S. Y.; Thompson, M. E.; Forrest, S. R. *Nano Lett.* **2010**, *10*, 3555–3559.
(21) Wei, G. D.; Wang, S. Y.; Renshaw, K.; Thompson, M. E.; Forrest, S. R. *ACS Nano* **2010**, *4*, 1927–1934.
(22) Wei, G.; Wang, S.; Sun, K.; Thompson, M. E.; Forrest, S. R. *Adv. Energy Mater.* **2011**, *1*, 184–187.
(23) Johns, J. E.; Muller, E. A.; Frechet, J. M. J.; Harris, C. B. *J. Am. Chem. Soc.* **2010**, *132*, 15720–15725.
(24) Hains, A. W.; Liang, Z. Q.; Woodhouse, M. A.; Gregg, B. A. *Chem. Rev.* **2010**, *110*, 6689–6735.
(25) Wu, C.; Djurovich, P. I.; Thompson, M. E. *Adv. Funct. Mater.* **2009**, *19*, 3157–3164.
(26) Emery, K. In *Handbook of Photovoltaic Science and Engineering*; Luque, A. H. S., Ed.; Wiley & Sons: Chichester, UK, 2003.
(27) Matson, R. J.; Emery, K. A.; Bird, R. E. *Sol. Cells* **1984**, *11*, 105–145.
(28) Shrotriya, V.; Li, G.; Yao, Y.; Moriarty, T.; Emery, K.; Yang, Y. *Adv. Funct. Mater.* **2006**, *16*, 2016–2023.
(29) Tian, M. Q.; Furuki, M.; Iwasa, I.; Sato, Y.; Pu, L. S.; Tatsuura, S. *J. Phys. Chem. B* **2002**, *106*, 4370–4376.
(30) Alleyne, B. D.; Bernard, L., St; Jaggernauth, H.; Hall, L. A.; Baxter, I.; White, A. J. P.; Williams, D. J. *Inorg. Chem.* **1999**, *38*, 3774–3778.
(31) Sprenger, H. E.; Ziegenbein, W. *Angew. Chem., Int. Ed.* **1966**, *5*, 894.
(32) Sprenger, H. E.; Ziegenbein, W. *Angew. Chem., Int. Ed.* **1968**, *7*, 530–535.
(33) Law, K. Y.; Bailey, F. C. *Can. J. Chem.* **1986**, *64*, 2267–2273.
(34) Louie, J.; Hartwig, J. F. *Tetrahedron Lett.* **1995**, *36*, 3609–3612.
(35) Hartwig, J. F.; Kawatsura, M.; Hauck, S. I.; Shaughnessy, K. H.; Alcazar-Roman, L. M. *J. Org. Chem.* **1999**, *64*, 5575–5580.
(36) Guram, A. S.; Rennels, R. A.; Buchwald, S. L. *Angew. Chem., Int. Ed.* **1995**, *34*, 1348–1350.

(37) McOmie, J. F. W.; Watts, M. L.; West, D. E. *Tetrahedron* **1968**, *24*, 2289–2292.
(38) Dirk, C. W.; Herndon, W. C.; Cervanteslee, F.; Selnau, H.; Martinez, S.; Kalamegham, P.; Tan, A.; Campos, G.; Velez, M.; Zyss, J.; Ledoux, I.; Cheng, L. T. *J. Am. Chem. Soc.* **1995**, *117*, 2214–2225.
(39) Ashwell, G. J.; Bahra, G. S.; Brown, C. R.; Hamilton, D. G.; Kennard, C. H. L.; Lynch, D. E. *J. Mater. Chem.* **1996**, *6*, 23–26.
(40) Lynch, D. E.; Byriel, K. A. *Cryst. Eng.* **1999**, *2*, 225–239.
(41) Curtis, M. D.; Cao, J.; Kampf, J. W. *J. Am. Chem. Soc.* **2004**, *126*, 4318–4328.
(42) Walker, B.; Kim, C.; Nguyen, T. Q. *Chem. Mater.* **2011**, *23*, 470–482.
(43) Gauger, J.; Manecke, G. *Chem. Ber.* **1970**, *103*, 2696–2706.
(44) Law, K. Y. *J. Phys. Chem.* **1987**, *91*, 5184–5193.
(45) Law, K. Y. *J. Photochem. Photobiol., A* **1994**, *84*, 123–132.
(46) Wolf, J.; Law, K.-Y.; Myers, A. B. *J. Phys. Chem.* **1996**, *100*, 11870–11882.
(47) Turro, N. J. *Modern Molecular Photochemistry*; Benjamin/Cummings: Menlo Park, CA, 1978.
(48) Cornelissen-Gude, C.; Rettig, W.; Lapouyade, R. *J. Phys. Chem. A* **1997**, *101*, 9673–9677.
(49) Rettig, W. *Angew. Chem., Int. Ed.* **1986**, *25*, 971–988.
(50) D'Andrade, B. W.; Datta, S.; Forrest, S. R.; Djurovich, P. I.; Polikarpov, E.; Thompson, M. E. *Org. Electron.* **2005**, *6*, 11–20.
(51) Djurovich, P. I.; Mayo, E. I.; Forrest, S. R.; Thompson, M. E. *Org. Electron.* **2009**, *10*, 515–520.
(52) Lassiter, B. E.; Wei, G.; Wang, S.; Zimmerman, J. D.; Diev, V. V.; Thompson, M. E.; Forrest, S. R. *Appl. Phys. Lett.* **2011**, *98*, 243307.